

Adsorption characteristics of NH₂-UiO-66 for the removal of hematite inorganic dye from industrial wastewater: Isotherm, thermodynamic, and kinetic study

Abbas Mohammadi^{1,2}
Mehdi Sedighi²

Abstract

Metal-organic frameworks (MOFs) have emerged as a class of highly promising materials for wastewater dye removal due to their unique properties. However, the existing body of research has primarily concentrated on the removal of organic dyes. To address this gap and contribute to advancements in water treatment technologies, this study investigates the efficacy of a zirconium-terephthalate-based MOF for the adsorptive removal of hematite, an inorganic dye, from aqueous environments. This investigation explored the influence of key parameters, including initial dye concentration, pH, adsorbent dosage, and adsorption temperature, on the adsorption capacity of NH₂-UiO-66 for hematite. The findings revealed that elevated temperatures and initial dye concentrations promoted hematite adsorption onto NH₂-UiO-66. Furthermore, the analysis of experimental data demonstrated concordance with the theoretical predictions of both the linearized Freundlich and Langmuir isotherm models. The study of kinetic models reveals that the pseudo-first-order model can adequately describe experimentally obtained data. The adsorption thermodynamic parameter ΔG_0 was found to be approximately -3.70, -3.94, and -4.19 kJ.mol⁻¹ at 298, 313, and 328 K, respectively. Furthermore, the ΔH_0 and ΔS_0 parameters were 5.15 kJ.mol⁻¹ and 54.3 J.mol⁻¹, respectively, indicating an endothermic adsorption mechanism. Further investigation found that the regeneration effectiveness is greater than 92% even after three adsorption cycles.

Keywords: Inorganic dye, hematite, adsorption, isotherm, metal–organic framework.

Received: 10 May 2024; Accepted: 10 July 2024

¹ Safety & Protection Research Center (S.P.R.C.), University of Qom, Qom, Iran, Email: Mohammadi.a@qom.ac.ir (Corresponding author)

² Department of Chemical Engineering, University of Qom, Qom, Iran.



1. Introduction

There has been a notable rise in the utilization of dyes across a wide range of industries in recent years. These industries include paper, petroleum, plastics, printing, cosmetics, textiles, leather, food, paint, rubber, pharmaceuticals, and dyestuffs. Residual dyes within industrial effluent present a substantial threat to human health and the environment. This risk stems from the inherent toxicity and carcinogenic properties of these dyes [1,2]. Dyes exhibit high resistance to degradation by heat, light, and oxidizing agents [3]. The presence of these pigmented pollutants not only detracts from the visual quality of water resources but also serves as a significant inhibitor of light penetration, thereby detrimentally impacting the photosynthetic processes of aquatic organisms [4]. As a result, one of today's most serious concerns is the treatment of dye-containing wastewater. Various physicochemical and biological methods, including adsorption [5-7], flocculation [8-10], electrolysis [11-13], coagulation [8,14,15], catalytic oxidation [16-18], ultra-filtration [19,20], and biodegradation [21,22], are employed for the removal of dyes. In the domain of water treatment, physical methods are increasingly favored over chemical and biological techniques due to their inherent economic benefits, operational simplicity, and minimal production of residual contaminants in the treated water [23,24]. Within the diverse spectrum of techniques employed for the remediation of wastewater harboring natural and synthetic dyes, adsorption has established itself as a frontrunner. This preeminence stems from its confluence of advantageous characteristics, including economic feasibility (manifested by low cost), remarkable efficacy in dye removal, broad applicability across a variety of dye types, minimal environmental footprint, and straightforward operational requirements [23,25].

Activated carbon, mesoporous silicates, zeolites, carbon nanotubes, diatomaceous earth, and resins are among the common adsorbents discussed in the literature. An effective adsorbent possesses several distinguishing features, including a high porosity with a substantial surface area, simplified preparation process, affordability, sturdy mechanical and thermal properties, impressive adsorption capabilities, and the capacity to regenerate over a broad spectrum of contaminants. Metal-organic frameworks (MOFs) emerge as a captivating class of novel materials demonstrating exceptional potential for dye removal applications. This efficacy can be ascribed to their remarkable stability and the vastness of their specific surface area [1]. By virtue of their facile synthesis, extensive surface areas, significant porosities, and tunable pore dimensions, these materials exhibit remarkable potential for diverse applications, encompassing adsorption, catalysis, detection, storage, and healthcare [26]. Much research has been conducted and published on employing MOFs for the removal of metals, anions, dyes, and various organics from polluted water [27,28]. Because of their outstanding water stability and excellent adsorption capabilities, zirconium (IV)-based MOFs have been reported to have adsorptive properties in these studies [23]. Since UiO-66, $\text{NH}_2\text{-UiO-66}$, $\text{N}_2\text{-UiO-66}$, and a number of other zirconium (Zr)-based MOF fulfill a wide range of the specific criteria, they have emerged as promising candidates for the treatment of water contaminated with dyes [1,3,24,29]. Chen et al. employed UiO-66 and $\text{NH}_2\text{-UiO-66}$ frameworks to assess their efficacy in adsorbing a range of hydrophilic dyes possessing both anionic and cationic functionalities [24]. Li et al. [30] explored the application of microwave-synthesized UiO-66 for the adsorptive removal of dyes. Their findings revealed a higher affinity of $\text{NH}_2\text{-UiO-66}$ (aminated UiO-66) for cationic dyes (Rhodamine B, Neutral Red, and Methylene Blue) compared to anionic dyes (Acid Chrome Blue K and Methyl Orange). This suggests a potential influence of electrostatic interactions on the adsorption process. He et al. [3] reported the elimination of Rhodamine B by adsorption on UiO-66. They also looked into the regeneration of used adsorbents and demonstrated that the material may be reused for six sorption/desorption cycles. A later investigation focused on UiO-66's ability to adsorb, or bind, Acid Orange 7 (AO7)

dye [31]. Embaby et al. [23] utilized an adsorption technique to assess the effectiveness of UiO-66 in removing a variety of organic dyes. Their study encompassed a broad spectrum of dyes, including both anionic (Methyl Orange, Eosin, and Alizarin Red S) and cationic varieties (Fuchsin Basic, Neutral Red, Safranin T, and Methylene Blue). Tambat et al. [32] investigated the effects of solution pH and initial Safranin dye concentration on the NH₂-UiO-66's capacity for adsorbing the dye. In their recent work, the authors synthesized UiO-66 and N₂-UiO-66 MOFs and assessed their potential for the adsorptive capture of a range of organic pollutants, including basic blue, red 2B, methyl orange, and acid green dyes [29].

Mousavi et al. [33] elucidated the adsorption behavior of UiO-66 materials they synthesized. Cationic dye methylene blue (MB) and anionic dye methyl red (MR) were chosen as model organics. In their study, Fang et al. explored the efficacy of Zr-based MOFs in removing methylene blue (MB), a cationic dye. They employed both solvothermal and microwave irradiation techniques for the synthesis of these MOFs [1]. Qui et al. [34] explored the application of acid-assisted synthesis for the fabrication of UiO-66, a metal-organic framework (MOF), exhibiting a marked selectivity towards the adsorption of anionic dyes (e.g., methyl orange) compared to cationic dyes (e.g., methylene blue).

Most research studies have focused on UiO-66 or NH₂-UiO-66 combined with organic dyes. However, NH₂-UiO-66's application in removing inorganic dyes through adsorption has been relatively overlooked. This study introduces the solvothermal synthesis of NH₂-UiO-66 and evaluates its efficacy in removing hematite (α -Fe₂O₃) dye. Hematite, owing to its abundant natural availability, serves as a widely utilized red mineral dye and holds significant economic importance as an inorganic red pigment. An extensive evaluation of NH₂-UiO-66's adsorption capacity for dye removal was undertaken. This comprehensive investigation explored the influence of initial dye concentration, adsorption temperature, adsorbent dosage, and solution pH. To elucidate the underlying adsorption mechanism, various isotherm models (Freundlich, Langmuir, Temkin, and Dubinin-Radushkevich) were employed in both linear and non-linear forms, achieving optimal data fitting. Additionally, kinetic models like pseudo-first and pseudo-second order, power law (Elovich), and Fick's law (intraparticle diffusion) were employed to gain insights into the adsorption rate process. Moreover, the thermodynamic parameters related to the adsorption mechanism were examined.

2. Experimental procedure

2.1. Materials

The Sigma-Aldrich company supplied 99.99% pure zirconium tetrachloride compounds and 99% pure 2-amino terephthalic acid. Merck company provided dimethyl-formamide (DMF), sodium hydroxide with a purity of more than 97%, and HCl with a purity of 37%. The absolute C₂H₅OH was also prepared by Kimia Alkol Company. Ishtar Company provided hematite powder.

2.2. Methods

Metal-organic framework (MOF) syntheses were carried out in either 25 mL or 100 mL vials. A commercial ultrasonic bath (Yaxun YX3080) was employed for ultrasonic irradiation during the synthesis process. Following synthesis, the as-prepared MOFs were dried in a vacuum oven (Memmert VO-200) to remove any residual solvent. The weight of each material was precisely determined using an analytical balance capable of measuring to 0.1 mg. The reaction mixtures were centrifuged using a general-purpose centrifuge (model 37852). Powder X-ray diffraction (PXRD) analysis was conducted on a commercially available diffractometer (ARL Thermo-Xray) operated at standard operating conditions (20 kV and 20 mA). FTIR spectra were collected in

wavenumbers (cm⁻¹) using KBr pellets on a commercially available spectrometer (Thermo/Nicolet Magna-IR 550). Brunauer-Emmett-Teller (BET) surface area analysis was performed with a modern instrument (NOVA E-series). Additionally, UV/Vis absorbance measurements were obtained using a commercial UV/Vis spectrometer (GBC UV/VIS 911A). Adsorption experiments were conducted within a 200 mL cylindrical glass vessel equipped with a water jacket to ensure a constant temperature for the adsorption process. The solution was continuously agitated using a JOANLAB LS-40PRO shaker. To eliminate any residual particulates, the dye solution was subsequently filtered through Durapore 0.22 μm filters. Precise temperature control was achieved by employing a Lauda RE-104 circulator. A Radiometer PHM250 ion analyzer was utilized to accurately measure the solution's pH through a potentiometric technique.

2.3. Adsorbent synthesis procedure

The ZrCl₄-based adsorbent was synthesized via a solvothermal method [1, 35] following these steps. A 23 mL vial containing 65 mg of ZrCl₄ and 5 mL of DMF was sonicated for 12 min. Subsequently, 0.5 mL of concentrated HCl, acting as a reaction catalyst, was introduced, and the mixture underwent further sonication for 10 minutes. To promote ligand complexation, 72 mg of H₂NC₆H₃-1,4-(CO₂H)₂ (ligand) and an additional 15 mL of DMF (solvent) were introduced to the vial. The resulting mixture was sonicated for 20 minutes to achieve complete dissolution of all precursors. Subsequently, the sealed vial was subjected to thermal activation at 100 °C for 2-3 hours, facilitating the formation of the desired white catalyst particles. The solid product was isolated through repeated washing with (CH₃)₂NC(O)H solvent and centrifugation (3000 rpm) to eliminate residual reaction media. The purified catalyst underwent further washing steps with absolute ethanol (C₂H₅OH) to replace the higher boiling point DMF solvent. This solvent exchange step promotes enhanced porosity and adsorption capacity within the final catalyst structure. Following adsorption, the solid phase was isolated once again through centrifugation at 3000 rpm. Subsequently, the recovered adsorbent was dried and its weight was determined under vacuum (30-40 mbar) at a temperature of 373 K. A detailed discussion on the optimization of NH₂-UiO-66 synthesis is provided in a previous publication by the authors [36].

2.4. Adsorption test procedure

A stock solution containing 500 parts per million of dye in deionized water (2000 mL) was synthesized. Samples were acquired by diluting the stock solution to the desired dye concentrations (40, 70, 100, and 130 ppm). The specified quantity of NH₂-UiO-66 adsorbent (at concentrations of 100, 300, and 500 ppm) was introduced into a 100 mL dye solution while maintaining continuous agitation on a shaker at 200 rpm. To ensure consistent temperature control during the adsorption process, a water circulation system was utilized. The experimental temperatures were set at 298 K, 313 K, and 325 K. The pH of the solution was meticulously adjusted using sodium hydroxide (NaOH) for alkaline conditions and hydrochloric acid (HCl) for acidic conditions, targeting specific values of 3, 7, and 10. Aliquots were withdrawn from the reaction mixture at predetermined time intervals for subsequent analysis. These samples were then filtered through a 0.22-micrometer membrane filter to remove the adsorbent particles. The absorbance of post-filtration samples was quantified using a UV-Vis spectrophotometer. Subsequently, dye concentration was ascertained by referencing a pre-constructed calibration curve. To guarantee data reliability, these measurements were replicated until consistent dye content was observed across a minimum of four consecutive samplings. Fig. 1 shows the reaction mixture at various stages of synthesis.

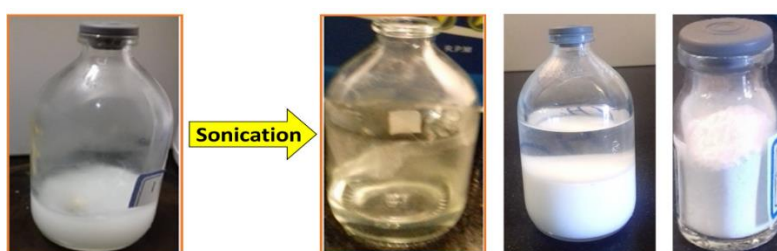


Figure 1. From left to right: zirconium tetrachloride suspension before entering and after leaving the ultrasonic bath, reaction mixture 12 hours after entering the oven (step out), washed and dried adsorbent

3. Results and Discussion

3.1. Characterization of the synthesized adsorbent

The X-ray diffraction (XRD) pattern of the synthesized $\text{NH}_2\text{-UiO-66}$ is depicted in Fig. 2. This pattern indicates the crystalline nature of the adsorbent and aligns with similar descriptions found in existing references [37,38]. The IR spectra of this adsorbent are depicted in Fig. 3. The IR spectrum of the produced catalyst corresponds to the spectra identified in the previously published references [37,38].

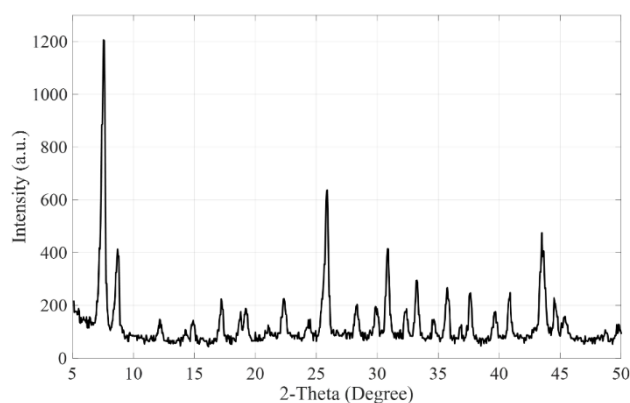


Figure 2. Powder XRD pattern of synthesized $\text{NH}_2\text{-UiO-66}$

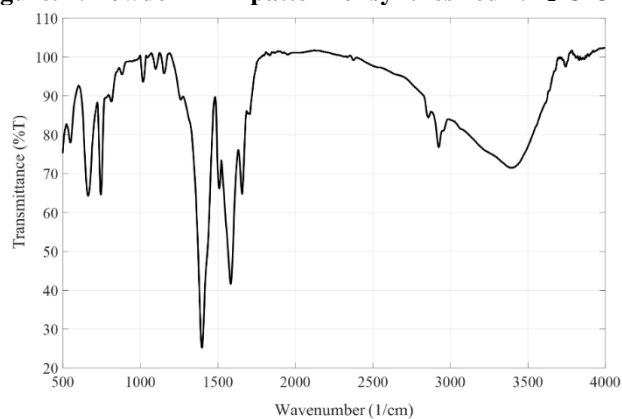


Figure 3. The IR spectrum of synthesized $\text{NH}_2\text{-UiO-66}$

Tambat et al. found significant peaks at wavenumbers of 3452, 3348, 2988, 1564, and 1381 cm⁻¹ [32]. Based on their research, the distinctive absorption spectra for NH₂-UiO-66 have been analyzed, and the absorption bands at 3449 cm⁻¹ and 3352 cm⁻¹ were determined as the result of stretching vibrations of the amine functional group, specifically the asymmetric and symmetric modes, respectively. Whereas, the absorption peak observed at 3002 cm⁻¹ corresponds with the C-H stretching mode associated with the physisorbed N, N-dimethylformamide. However, the major absorption peaks for carboxylic acid functional groups at 1558 cm⁻¹ and 1368 cm⁻¹ are attributed to the symmetric and asymmetric stretching vibrations, respectively. In the present study, these peaks were detected at wavenumbers 3748, 3399, 2921, 1582 cm⁻¹, and 1401 cm⁻¹, aligning with the findings reported by Tambat [32]. Based on the BET analysis, the synthesized adsorbent exhibits an approximate specific surface area of 825 m²/g, a total pore volume of 0.463 cm³/g, and a mean pore diameter of 22.46 Å. Fang et al. [1] reported contrasting values for their solvothermally synthesized NH₂-UiO-66: a specific surface area of 509 m²/g, a pore volume of 0.252 cm³/g, and a mean pore diameter of 19.79 Å. These values differ slightly from those obtained in the present study.

3.2. Effect of initial dye concentration

To examine the effect of dye concentration on adsorption capacity, this research employed a range of concentration levels: 40 ppm, 70 ppm, 100 ppm, and 130 ppm. To isolate this effect, all other parameters were rigorously controlled. A constant adsorbent dosage of 300 ppm, an adsorption temperature of 298 K, and the natural solution pH were maintained across all experiments. Interestingly, the as-prepared hematite dye solutions (40-130 ppm) inherently possessed a natural pH. The findings pertaining to the correlation between adsorption capacity (Q_t) and contact time (t) are presented in Fig. 4. The following equation was utilized to calculate the adsorption capacity:

$$Q_t = (C_i - C_t)(V/M) \quad (1)$$

where C_i (ppm) and C_t (ppm) symbolize the initial and time-dependent dye concentrations, respectively. V (L) represents the solution volume, and M (g) denotes the mass of the employed adsorbent. The ability to adsorb increases with higher dye concentrations. In accordance with the findings of Fang et al. [1], the increase in the initial concentration of methylene blue dye results in an augmented adsorption capacity for NH₂-UiO-66. This phenomenon is interpreted as an intensification of the concentration gradient effect. This interpretation is bolstered by the findings of Tambat et al. [32] and Li et al. [30]. These studies observed consistent dye removal patterns for Safranin and Acid Chrome Blue K dyes, respectively, using both NH₂-UiO-66 and UiO-66. Based on this alignment with prior research, the present investigation focuses on the adsorption of Safranin onto NH₂-UiO-66. The increased adsorption capacity can be ascribed to a more pronounced concentration gradient, which promotes a more efficient mass transfer process between the adsorbent (NH₂-UiO-66) and the adsorbate (Safranin dye). As illustrated in the accompanying figure, the equilibrium adsorption capacity (Q_e) exhibits a positive correlation with increasing initial dye solution concentrations (40, 70, 100, and 130 ppm), reaching values of 121, 145, 186, and 241 mg·g⁻¹, respectively. Equilibrium adsorption capacity (Q_e) demonstrates a near-linear dependence on the initial dye concentration, as

corroborated by a high linear regression correlation coefficient ($R^2 = 0.981$). This observation aligns with the previous work of Tambat et al. [32], which reported the effectiveness of $\text{NH}_2\text{-UiO-66}$ in removing Safranin dye from aqueous solution.

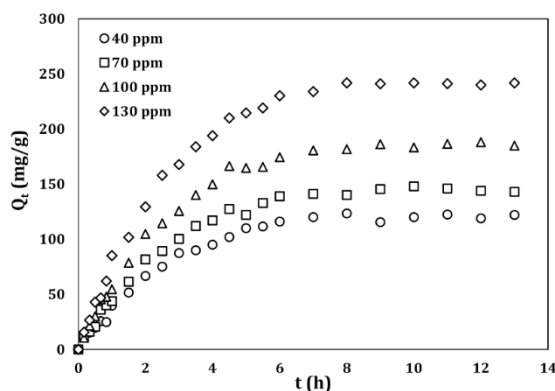


Figure 4. Adsorption capacity variation with changes in Dye Concentration at $T=298\text{ K}$, $\text{MOF}=300\text{ ppm}$, $\text{pH}=7$

3.3. Effect of the amount of $\text{NH}_2\text{-UiO-66}$

Fig. 5 shows a plot of Q_t vs contact time for various adsorbent quantities. In this study, the amount of MOF was in the range of 100-500 ppm, with three levels (100, 300, and 500 ppm). Fig. 5 shows an inset of a sample solution before and after adsorption, which became practically colorless after 13 hours. A positive correlation was observed between the adsorbate quantity (Q_t) and the adsorbent mass, indicating a direct relationship between available adsorption sites and contaminant uptake. This aligns with the observations reported by Fang et al. [1] during the adsorption and removal of methylene blue (MB), a positively charged dye, using $\text{NH}_2\text{-UiO-66}$ as the adsorbent. Furthermore, employing a minimal adsorbent dosage (100 ppm) necessitated an extended equilibration time exceeding 22 hours. In contrast, a larger amount of adsorbent material (500 ppm) reached equilibrium within just 4 hours, highlighting rapid adsorption of the dye. This is owing to increased site availability and the enhanced possibility of dye collection from aqueous solution. The equilibrium adsorption capacity (Q_e) values exhibited a positive correlation with increasing $\text{NH}_2\text{-UiO-66}$ adsorbent concentrations (100, 300, and 500 ppm), reaching values of 131, 186, and 190 mg. g^{-1} , respectively. However, the observed increase in Q_e plateaued at higher adsorbent dosages (300 ppm), suggesting a diminishing return effect on adsorption capacity with further increases in $\text{NH}_2\text{-UiO-66}$ concentration. This can be attributed to the availability of more active binding sites on the adsorbent surface at the higher dosage. Meanwhile, because the solution under test contains a limited number of pigment particles, increasing the number of accessible active sites from 300 to 500 ppm will no longer result in a significant rise in Q_e value. As a result, the upper limit of this variable has been set at 500 ppm.

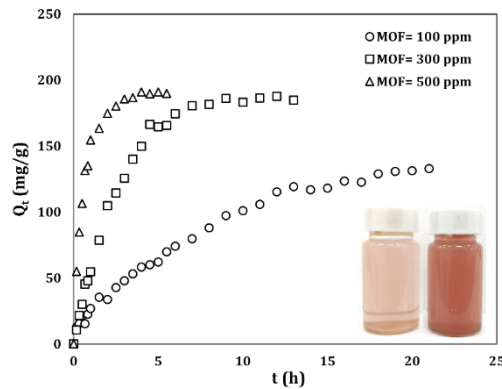


Figure 5. The effect of NH₂-UiO-66 amount on adsorption capacity ($T=298$ K, $C_i=100$ ppm, and $pH=7$). The inset: a sample solution before and after adsorption, which became nearly colorless after 13 hours.

3.4. Effect of adsorption temperature

Fig. 6 illustrates a pronounced dependence of the equilibrium adsorption capacity (Q_t) for hematite adsorption onto NH₂-UiO-66 on the employed temperature. The data reveal a clear and consistent increase in Q_t with increasing temperature, from 298 K to 313 K and further to 328 K. This observation aligns with the findings reported by He et al. [3] for the adsorption of Rhodamine B dye onto UiO-66. This alignment suggests a potentially analogous underlying mechanism governing the temperature-dependent adsorption behavior in the present system. As shown in Fig. 6, the equilibrium capacities at 298, 313, and 328 K are 186, 250, and 290 mg.g⁻¹, respectively. These results point to an endothermic adsorption process. Higher temperatures improve dye molecule transfer into adsorbent particle surfaces by enhancing dye molecule diffusion across the external boundary layer and decreasing solution viscosity. At lower temperatures (298 K), it took more than 9 hours for the Q_t value to reach equilibrium, while at higher temperatures (328 K), the Q_t value reached equilibrium in about 3 hours. This indicates that dye molecule diffusion and adsorption are faster at higher temperatures.

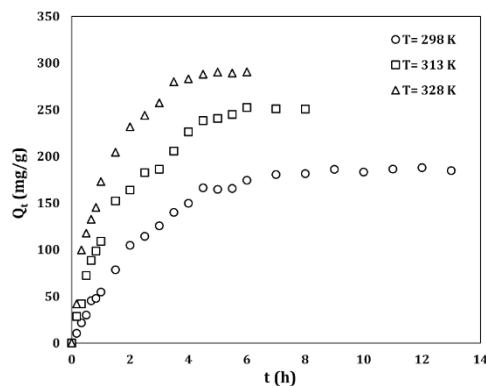


Figure 6. The effect of temperature effect on adsorption capacity ($C_i=100$ ppm, MOF=300 ppm, and $pH=7$).

3.5. Effect of solution pH

In adsorption processes, the pH of the system is a critical parameter as it alters the zeta potential (surface electric charge) of the adsorbent material. This study systematically investigated the effect of pH on the adsorption process over the range of 3 to 10, with three discrete levels (3, 7, and 10) examined. Fig. 7 depicts the relationship between the equilibrium adsorption capacity (Q_t) and the contact time at these varying pH conditions. The observed trends closely mirror those identified previously in Fig. 4 (initial dye concentration) and Fig. 6 (adsorption temperature), suggesting a potential underlying influence of pH on the adsorption mechanism. The corresponding equilibrium adsorption capacities (Q_e) at the three pH levels were 47, 186, and 79 mg. g⁻¹, respectively, with the maximum adsorption occurring at the neutral pH of 7. The results presented herein emphatically demonstrate the critical role of pH in regulating the adsorption performance of the employed adsorbent material.

The observed maximum equilibrium adsorption capacity (Q_e) at neutral pH is due to fluctuations in the surface charge of NH₂-UiO-66, as shown by its zeta potential (ZP) over the pH range studied. Tambat et al. found that the ZP of NH₂-UiO-66 is negative at pH = 10 (-25 mV), generally steady at pH = 7 (-24 mV), and positive at pH = 3 (8 mV), with a point of zero charge (PZC) at pH = 3.5 [32]. The surface charge properties of NH₂-UiO-66, as defined by its ZP, have been shown to vary with pH. At pH values exceeding 3.5, the adsorbent exhibits a negative charge, while it becomes positively charged at lower pH (below 3.5). Therefore, a comprehensive investigation of the adsorbent's surface charge, as measured by zeta potential, is crucial for elucidating the adsorption behavior of hematite pigments onto NH₂-UiO-66 across a broad pH range. It is noteworthy that existing data on this subject demonstrates significant inconsistencies. Forbes and Franks found that the ZP of hematite at 298 K and pH values of 10, 7, and 3 were -10, +20, and more than +55 mV, respectively [39]. Abaka-Wood et al. reported that the ZP value of hematite at pH values of 10, 7, and 3 were -8, zero, and +19 mV, respectively [40]. Yang et al. reported that the zeta potential of hematite at pH values of 10, 7, and 3 were -32, -20, and +5 mV, respectively [41]. Fan et al. [42] reported these values as -8, zero, and +20 mV, which are similar to the values reported by Abaka-Wood et al. [40]. Shrimali et al. reported that the ZP values of hematite at pH values of 10, 7, and 3 were less than -60, -16, and +40 mV, respectively [43]. The high dispersion of available data may be due to the variety of hematite dyes and the difference in the amount and type of impurities associated with this pigment. Hematite is a natural mineral pigment that is obtained primarily from natural sources, which is the primary reason for the high variability in the data.

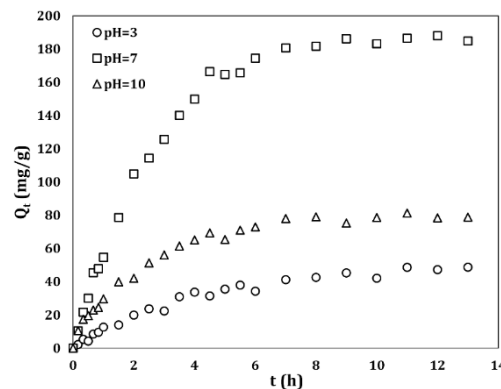


Figure 7. The effect of solution pH on adsorption capacity ($C_i=100$ ppm, MOF=300 ppm, and $T=298$ K).

The findings in Fig. 7 are consistent with the zeta potential values reported by Forbes and Franks [39]. Tambat et al. also reported the ZP of the adsorbent at pH values of 10, 7, and 3 as -25, -24, and +8, respectively [32]. According to Forbes and Franks [39], this indicates that at pH=10 (-25 and -10 mV) and pH=3 (+8 and > +55), the adsorbent and pigment have the same surface charge. However, at pH=7, the surface charges of the adsorbent and pigment have opposite signs (+20 and -24), which leads to a more efficient adsorption process than at the previous two pHs (as shown in Fig. 7). The optimal fulfillment of this separation process's operational, economic, and environmental considerations is indicated by the absence of extremely acidic and alkaline operating conditions, as well as the presence of extreme adsorption capacity around neutral pH.

3.6. Effect of adsorbent regeneration

In accordance with the aforementioned criteria for an ideal adsorbent, its reusability was investigated. This involved evaluating the regeneration and material recycling of the used adsorbent over four sorption-desorption cycles. To achieve this, the post-sorption material was isolated using a Dura-pore 0.22 μm filter, followed by a washing step and drying at 100 °C under a vacuum pressure of 30-40 mbar. Following meticulous regeneration using a 0.01 N sodium hydroxide solution, as described by Tambat et al. [32, 44], the NH₂-UiO-66 MOF was desiccated under reduced pressure at 100 °C within an electric oven. Subsequent adsorption cycles employed the regenerated MOF. As depicted in Fig. 8, the NH₂-UiO-66 exhibited exceptional regeneration efficiency, consistently exceeding 92% across multiple cycles. This observation signifies the remarkable reusability of the NH₂-UiO-66 MOF, maintaining a consistent adsorption capacity for at least three regeneration cycles.

3.7. Adsorption isotherms

Experimental adsorption equilibrium data were analyzed using four prominent adsorption isotherm models. The suitability of these models was evaluated comparatively through the calculation of their corresponding correlation coefficient (R^2) values. Table 1 presents the non-linear and linearized forms of the employed isotherm equations, as derived from references [45] and [46]. Notably, within these equations, Q_m represents the theoretical maximum adsorption capacity ($\text{mg}\cdot\text{g}^{-1}$), while C_0 and C_e designate the initial and equilibrium hematite concentrations ($\text{mg}\cdot\text{L}^{-1}$), respectively.

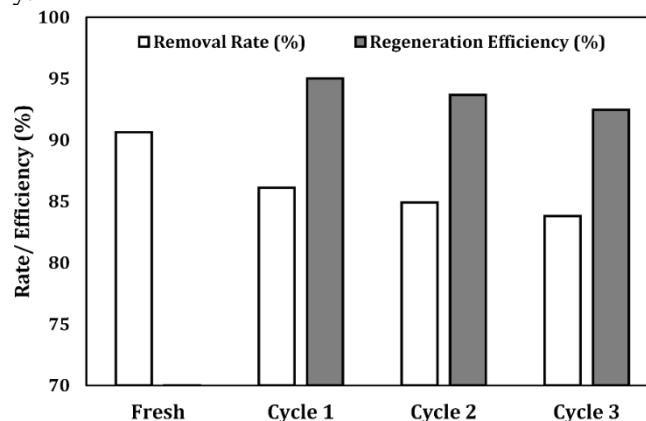


Figure 8. The removal rate and regeneration efficiency of hematite on NH₂-UiO-66 at different adsorption cycles ($C_i=40$ ppm, MOF=300 ppm, pH=7, and T=298 K).

Table 1. Analysis of the non-linear and linearized equations for various adsorption isotherm models [45,46]

Isotherm model	Linear equation	Non-linear equation	Separation factor (favorability of the adsorption)
Langmuir	$\frac{C_e}{Q_e} = \frac{1}{K_L Q_m} + \frac{C_e}{Q_m}$	$Q_e = \frac{K_L Q_m C_e}{(1 + K_L C_e)}$	$R_L = \frac{1}{(1 + K_L C_0)}$
Freundlich	$\ln(Q_e) = \frac{1}{n} \ln(C_e) + \ln(K_F)$	$Q_e = K_F C_e^{1/n}$	$1/n$
Temkin	$Q_e = \frac{RT}{K_T} \ln(C_e) + \frac{RT}{K_T} \ln(A_T)$	$Q_e = \frac{RT}{K_T} \ln(A_T C_e)$	---
Dubinin-Radushkevich	$\ln(Q_e) = \ln(Q_s) - K \varepsilon^2$ where $\varepsilon = RT \ln\left(1 + \frac{1}{C_e}\right)$		---

Within the Langmuir isotherm framework, the Langmuir constant (K_L , L mg⁻¹), is employed to quantify the rate of adsorption. The dimensionless separation factor (R_L) serves to evaluate the efficacy of the adsorption procedure. A favorable adsorption outcome is indicated by a value of R_L within the range of 0 to 1. In contrast, R_L values that surpass 1 signify an unfavorable adsorption process, whereas a value of zero denotes an irreversible adsorption condition [29]. Within the Freundlich isotherm equation, K_F and n represent adsorption capacity and process favorability, respectively. The value of n^{-1} serves as an indicator of the isotherm type. Specifically, $n^{-1} = 0$ signifies irreversible adsorption, $0 < n^{-1} < 1$ indicates favorable adsorption conditions, and $n^{-1} > 1$ suggests unfavorable adsorption [29]. Within the Temkin isotherm model, the parameter A_T represents the equilibrium binding constant. K_T represents the constant correlated with fluctuations in adsorption energy. In contrast, the Dubinin-Radushkevich model introduces K as the adsorption energy constant, and ε as the Polanyi potential [45]. Table 2 presents a summary of the fitting R^2 values and their corresponding isotherm constants. A graphical depiction of these results is provided in Fig. 9. The Langmuir isotherm model postulates a monolayer adsorption process on a homogeneous surface with a finite number of non-interacting sites. This model signifies the formation of a single layer of adsorbates. In this study, the linear Langmuir isotherm yielded the highest R^2 value of 0.88 compared to other evaluated isotherm models, indicating its superior capacity to represent the experimental data. Furthermore, the separation factor (R_L) values calculated for initial dye concentrations (40, 70, 100, and 130 ppm) ranged from 0.208 to 0.075, indicating favorable adsorption across the concentration range. Consequently, the Langmuir model is inferred to be the most appropriate representation of the adsorption process, with the data following a linear Langmuir isotherm. Conversely, the non-linear Langmuir isotherm yielded a considerably lower R^2 value (0.55), signifying a poor fit for the current data set. However, the R_L values (0.025 - 0.078) obtained for the non-linear Langmuir model still indicate a favorable adsorption isotherm. The Freundlich isotherm, on the other hand, provides a well-established framework for analyzing adsorption processes on heterogeneous surfaces where multi-layer coverage can occur. This phenomenon is attributed to the inherent energetic variability of active sites and interactions between adsorbed molecules, as corroborated by reference [23]. The applicability of the Freundlich isotherm in this study was evaluated through linear and non-linear regression analyses, yielding R-squared values of 0.77 and 0.75, respectively. The results of the experimental data indicate a relatively satisfactory correspondence between the modeled outputs

and the empirically observed values. Furthermore, the estimates of the separation factor values for both the linear and non-linear forms of the isotherm were situated within the range of 0-1 (interval of 0.213 and 0.260), denoting advantageous adsorption conditions.

The Temkin isotherm, explored by [32], incorporates the influence of indirect interactions between adsorbate molecules on the adsorption isotherm. However, the correlation coefficients (R^2) of 0.69, presented in Table 2 for both linear and non-linear forms of this model, suggest a moderate fit at best with the experimental data. Similarly, the Dubinin-Radushkevich isotherm, which accounts for inherent sorbent properties and energy transfer during adsorption, exhibits an inadequate fit to the data. This is reflected by its corresponding correlation coefficient of 0.54.

Table 2. The calculated constants of the studied isotherm

Model		Constants					
Langmuir	Linear	Q_m (mg/g)	250.0	R_L	0.208 for $C_0= 40$ ppm		
		K_L (L/mg)	0.095		0.130 for $C_0= 70$ ppm		
		R^2	0.88		0.095 for $C_0= 100$ ppm		
	Non-linear	Q_m (mg/g)	210.3		0.075 for $C_0= 130$ ppm		
		K_L (L/mg)	0.296		0.078 for $C_0= 40$ ppm		
		R^2	0.55		0.046 for $C_0= 70$ ppm		
Freundlich	Linear	K_F (mg/g)	86.392	n^{-1}	0.213		
		n	4.701				
		R^2	0.77				
	Non-linear	K_F (mg/g)	74.330			n^{-1}	0.260
		n	3.849				
		R^2	0.75				
Temkin (T=298 K)	Linear	K_T (L/mg)		70.208			
		A_T		6.041			
		R^2		0.69			
	Non-linear	K_T (L/mg)		70.210			
		A_T		6.042			
		R^2		0.69			
Dubinin-Radushkevich	K		1.303E-6				
	Q_s (mg/g)		188.1				
		R^2		0.54			

Evaluation of the model fitting for the experimental equilibrium adsorption data of hematite onto NH₂-UiO-66 revealed that the linear Langmuir, linear Freundlich, and non-linear Freundlich models exhibited a superior fit compared to other models, as evidenced by their comparatively higher R^2 values. However, amongst these three, the linear Langmuir model emerged as the most favorable choice. This observation aligns with prior research, such as the work of He et al. on the adsorption of Rhodamine B dye onto UiO-66 [3]. Selecting an appropriate isotherm model is crucial for characterizing the adsorption equilibrium of this Zr-incorporated metal-organic framework (MOF). As evidenced by the presented regression coefficients, both the Langmuir and Freundlich models demonstrate efficacy in depicting the adsorption process on this MOF substrate. This aligns with findings from Embaby et al. [23], where anionic dyes displayed Langmuir isotherm behavior during adsorption onto UiO-66. Conversely, Tambat et al. [32] and Fang et al. [1] observed that the adsorption of cationic dyes onto NH₂-UiO-66 materials aligns

more closely with the Freundlich isotherm. It is also noteworthy that Molavi et al. investigated the adsorption of methyl orange and methylene blue dyes onto prepared UiO-66 [35]. The applicability of the Freundlich adsorption isotherm for both anionic and cationic dye adsorption mechanisms suggests a minimal interaction between adsorbate molecules. This, coupled with the observed adsorption behavior on NH₂-UiO-66 as depicted in the preceding data, lends credence to the hypothesis of monolayer adsorption. Furthermore, the suitability of the Langmuir adsorption model implies a homogeneity of sorption sites, signifying that the occupation of neighboring sites does not influence the individual adsorbate's binding affinity.

3.8. Adsorption kinetics

To elucidate the fundamental mechanism governing hematite pigment adsorption and the interactions occurring at the solid-liquid interface, a kinetic analysis was conducted. This investigation serves to identify the rate-determining step of the adsorption process. It is well recognized that various factors can influence adsorption mechanisms, such as mass transfer limitations at the interface, interfacial chemical reactions, and intra-particle diffusion within the adsorbent. To clarify the governing kinetic mechanism of the adsorption process, the experimental data were analyzed by fitting with four kinetic models. Specifically, the pseudo-first-order, pseudo-second-order, Elovich, and intraparticle diffusion models were employed, and their corresponding mathematical expressions are presented as detailed below [29]:

$$\ln(Q_e - Q_t) = \ln(Q_e) - k_1 t \quad (2)$$

$$\frac{t}{Q_t} = \frac{1}{k_2 Q_e^2} + \frac{t}{Q_e} \quad (3)$$

$$Q_t = \frac{1}{\beta} \ln(\alpha\beta) + \frac{1}{\beta} \ln(t) \quad (4)$$

$$Q_t = k_3 + k_4 t^{\frac{1}{2}} \quad (5)$$

Kinetic models are characterized by rate constants, k_1 (h⁻¹) and k_2 (g·mg⁻¹·h⁻¹), respectively. The Elovich equation incorporates additional parameters, α (mg·g⁻¹·h⁻¹) and β (g·mg⁻¹), representing the initial adsorption rate and desorption constant, respectively. Furthermore, k_3 (mg·g⁻¹·h^{-0.5}) and k_4 (mg·g⁻¹·h^{-0.5}) account for the influence of boundary layer thickness on the intra-particle diffusion rate and boundary layer resistance, respectively. Fig. 10 presents the linearized forms of the investigated kinetic models, corresponding to equations (2) to (5). The R² values and all model parameter values are additionally provided in Table 3.

Kinetic modeling of the adsorption process revealed that pseudo-order n models (encompassing both first and second-order) provided the most suitable fit for the empirical data. However, the pseudo-second-order model exhibited a superior performance, evident from its calculated equilibrium adsorption capacity (Q_e^{Cal}) closely aligning with the experimentally determined Q_e^{Exp} . Conversely, the intraparticle diffusion model displayed the lowest coefficient of determination ($R^2 = 0.91$), signifying its inadequacy. Internal diffusion models propose that the rate-determining step in adsorption can be attributed to mass transfer limitations within the adsorbent particle, often characterized by a low intraparticle diffusion coefficient. As demonstrated in Section 3.1, the synthesized NH₂-

UiO-66 exhibits a significant mean pore diameter (22.46 Å), surpassing the size of any employed dye molecule as reported in reference [29].

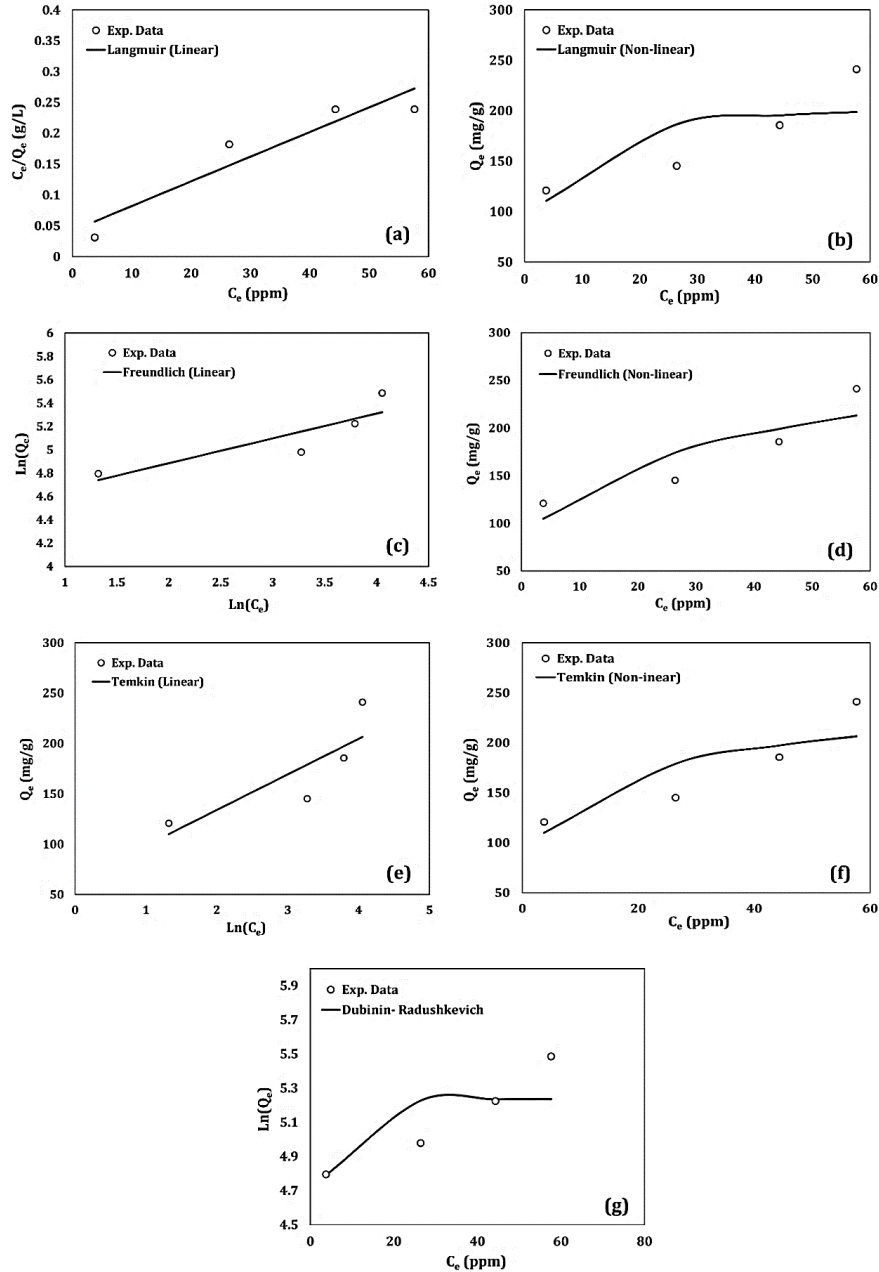


Figure 9. The presentation of regression graphs for hematite adsorption on NH₂-UiO-66: linear fittings (a, c, e) and non-linear fittings (b, d, f, g).

This translates to unhindered diffusion of dye molecules throughout the adsorbent's pores, effectively eliminating this phenomenon as the rate-limiting factor. This

observation aligns perfectly with the observed poor fit ($R^2 = 0.91$) of the intraparticle diffusion model when applied to the experimental data.

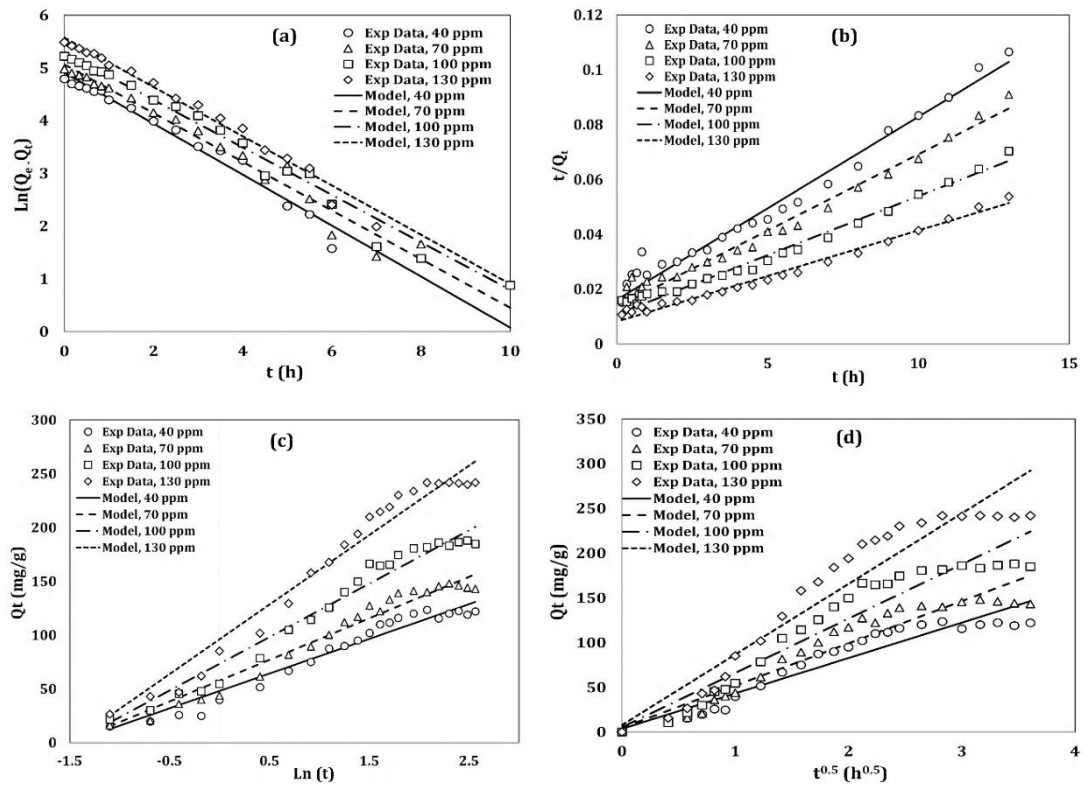


Figure 10. The plot of (a) Pseudo first-order, (b) Pseudo second-order, (c) Elovich, and (d) Intra-particle diffusion kinetic models.

An R^2 value of 0.96 obtained for the Elovich model suggests a relatively weak correlation, implying that this model may not be the most suitable for describing the adsorption behavior of hematite onto $\text{NH}_2\text{-UiO-66}$. The Elovich equation is typically employed in adsorption kinetics to characterize chemical adsorption mechanisms. Consequently, the findings of this study favor a physical rather than a chemical adsorption process for hematite on $\text{NH}_2\text{-UiO-66}$.

Table 3. The kinetic constants of hematite adsorption on NH₂-

Items	Q _e ^{Exp}	Q _e ^{Cal}	k ₁ (h ⁻¹)	k ₂ (g.mg ⁻¹ .h ⁻¹)	α (mg.g ⁻¹ .h ⁻¹)	β(g.mg ⁻¹)	k ₃ (mg.g ⁻¹ .h ^{-0.5})	k ₄ (mg.g ⁻¹ .h ^{-0.5})	R ²	Ave. R ²
Pseudo first-order model										
C ₀ =40 ppm	121	136	0.4833	---	---	---	---	---	0.97	
C ₀ =70 ppm	145	158	0.4613	---	---	---	---	---	0.97	0.98
C ₀ =100	186	199	0.4499	---	---	---	---	---	0.98	
C ₀ =130	241	263	0.4669	---	---	---	---	---	0.98	
Pseudo second-order model										
C ₀ =40 ppm	121	150	---	0.0028	---	---	---	---	0.96	
C ₀ =70 ppm	145	180	---	0.0023	---	---	---	---	0.97	0.97
C ₀ =100	186	232	---	0.0017	---	---	---	---	0.97	
C ₀ =130	241	301	---	0.0014	---	---	---	---	0.97	
Elovich model										
C ₀ =40	121	---	---	---	143	0.0310	---	---	0.95	
C ₀ =70 ppm	145	---	---	---	171	0.0259	---	---	0.96	0.96
C ₀ =100	186	---	---	---	217	0.0201	---	---	0.97	
C ₀ =130	241	---	---	---	285	0.0155	---	---	0.96	
Intraparticle diffusion model										
C ₀ =40 ppm	121	---	---	---	---	---	3.64	39.54	0.91	
C ₀ =70 ppm	145	---	---	---	---	---	4.69	47.22	0.91	0.91
C ₀ =100	186	---	---	---	---	---	5.34	60.69	0.92	
C ₀ =130	241	---	---	---	---	---	7.73	78.89	0.91	



3.9. Thermodynamic study

The thermodynamic behavior of this system was studied using the following equations:

$$\ln(K_F) = \frac{\Delta S_0}{R} - \frac{\Delta H_0}{RT} \quad (6)$$

$$\Delta G_0 = -RT \ln(K_F) \quad (7)$$

K_F denotes the Freundlich constant ($\text{mg} \cdot \text{g}^{-1}$) and T denotes temperature (K). Table 4 shows the thermodynamic parameters for the tested temperatures. Negative ΔG_0 results illustrate the process's viability and the adsorption's spontaneous behavior at the temperatures examined [3]. Thermodynamic analysis reinforces the observations presented in Fig. 6. The decreasing ΔG_0 with increasing temperature signifies a more favorable adsorption process at higher temperatures. This aligns well with the endothermic nature of hematite adsorption onto $\text{NH}_2\text{-UiO-66}$, as indicated by the positive ΔH_0 value ($5.149 \text{ kJ} \cdot \text{mol}^{-1}$). Furthermore, this ΔH_0 value falls within the range reported by Kara et al. [47] and He et al. [3] for physical adsorption (less than $40 \text{ kJ} \cdot \text{mol}^{-1}$). In conjunction with the results obtained from kinetic modeling experiments, the aforementioned thermodynamic data provides compelling evidence that the adsorption of hematite onto $\text{NH}_2\text{-UiO-66}$ occurs via a physisorption mechanism.

Table 4. The determination of thermodynamic properties for the sorption of hematite on $\text{NH}_2\text{-UiO-66}$ surface.

T (K)	K_F (mg/g)	ΔG_0 (J/mol)	ΔH_0 (J/mol)	ΔS_0 (J/mol.K)
298	86.39	-3703.7		
313	94.26	-3940.5	5148.9	54.3
328	104.52	-4190.7		

4. Conclusion

Metal-organic frameworks (MOFs) have emerged as a prominent class of materials for wastewater dye remediation due to their exceptional properties. Their potential applications in this area have been elucidated due to their unique characteristics. However, the existing literature predominantly focuses on the removal of organic dyes. This study reports the solvothermal synthesis of $\text{NH}_2\text{-UiO-66}$ and investigates the impact of four operational parameters on its capacity to adsorb hematite, an inorganic pigment. These parameters include dye concentration, adsorption temperature, adsorbent dosage, and solution pH. The experimental results demonstrate the effectiveness of $\text{NH}_2\text{-UiO-66}$ in hematite removal. The adsorption equilibrium was effectively modeled by both the linear Freundlich and Langmuir isotherms, with the latter exhibiting a superior fit. The pseudo-first-order model yielded an equilibrium adsorption capacity that closely mirrored the experimental values, suggesting a dominance of this kinetic mechanism. Furthermore, a positive correlation was observed between adsorption capacity and both temperature and initial dye concentration, suggesting a physisorption mechanism. This observation was complemented by the study's quantification of equilibrium constants, adsorption capacities, and thermodynamic parameters. Notably, the regeneration efficiency remained remarkably high ($> 92\%$) even after three adsorption cycles, indicating excellent reusability of the $\text{NH}_2\text{-UiO-66}$ adsorbent with minimal performance degradation.

References

1. Fang Y, Zhang L, Zhao Q, Wang X, Jia X, (2019). Application of acid-promoted UiO-66-NH₂ MOFs in the treatment of wastewater containing methylene blue. *Chemical Papers*, pp: 73:1401-1411.
2. Zeng L, Xiao L, Long Y, Shi X, (2018). Trichloroacetic acid-modulated synthesis of polyoxometalate@UiO-66 for selective adsorption of cationic dyes. *J. Colloid Interface Sci.*, pp: 516:274–283.
3. He Q, Chen Q, Lü M, Liu X, (2014). Adsorption behavior of rhodamine B on UiO-66. *Chin. J. Chem. Eng.*, pp: 22:1285–1290.
4. Roopaei H, Zohdi AR, Abbasi Z, Bazrafkan M, (2014). Preparation of new photocatalyst for removal of alizarin red-s from aqueous solution. *Indian Journal of Science and Technology*, pp: 7:1882–1887.
5. Gneedy AH, Dryaz AR, Said MSh, AlMohamadi HA, Ahmed SA, Elsayed R, Soliman NK, (2022). Application of marine algae separate and in combination with natural zeolite in dye adsorption from wastewater: a review, *Egyptian Journal of Chemistry*, pp: 65:589-616.
6. Sağlam S, Türk FN, Arslanoğlu H, (2023). Use and applications of metal-organic frameworks (MOF) in dye adsorption: review. *Journal of Environmental Chemical Engineering*, pp: 11: 110568.
7. Lan D, Zhu H, Zhang J, Li Sh, Chen Q, Wang Ch, Wu T, Xu M, (2022). Adsorptive removal of organic dyes via porous materials for wastewater treatment in recent decades: a review on species, mechanisms and perspectives. *Chemosphere*, pp: 293:133464.
8. De Sousa SR, Rengel HD, Voigt FD, Machado RAF, De Fátima MR, Marangoni C, (2023) Treatment of real textile wastewater by coagulation/flocculation integrated with direct contact membrane distillation. *Separation Science and Technology*, pp: 58:2394-2410.
9. Wang H, Song J, Yan M, Li J, Yang J, Huang M, Zhang R, (2023). Waste lignin-based cationic flocculants treating dyeing wastewater: fabrication, performance, and mechanism. *Science of The Total Environment*, pp: 874:162383.
10. Kolya H, Kang CW, (2023). Bio-based polymeric flocculants and adsorbents for wastewater treatment. *Sustainability*, pp: 15:1-36.
11. Asath Murphy MS, Jovitha Jane D, Sahaya LS, Robin RS, Palanichamy J, Kalivel P, (2023). Electrochemical treatment of textile wastewater using copper electrodes. *J Environ Sci Health A Tox Hazard Subst Environ Eng*, pp: 58:971-980.
12. Chen Zh, Feng M, Wang Y, Ma Q, Yin Q, (2023) Construction of a novel magnetic levitation iron-carbon micro-electrolysis treatment system for dye wastewater and its anti-passivation strategy. *Environ. Sci.: Water Res. Technol.*, pp: 9:2076-2088.
13. Xie J, Zou X, Chang Y, Xie J, Liu H, Cui MH, Zhang TC, Chen C, (2023). The microbial synergy and response mechanisms of hydrolysis-acidification combined microbial electrolysis cell system with stainless-steel cathode for textile-dyeing wastewater treatment. *Sci Total Environ.*, pp:10:158912.
14. Mim S, Hashem MA, Payel S, (2023). Coagulation-adsorption-oxidation for removing dyes from tannery wastewater. *Environ Monit Assess.*, pp:195: article number 695.
15. Sudirgo MM, Surya RA, Kristianto H, Prasetyo S, Sugih AK, (2023). Application of xanthan gum as coagulant-aid for decolorization of synthetic congo red wastewater. *Heliyon*, pp: 9: e15011.

16. Yu H, Liu Y, Cong Sh, Xia Sh, Zou D, (2023). Review of Mo-based materials in heterogeneous catalytic oxidation for wastewater purification. *Separation and Purification Technology*, pp: 312:123345.
17. Shokoohi R, Godini K, Latifi Z, (2023). Catalytic Oxidation of reactive blue 222 dye using peroxy monosulfate activated by Mn_3O_4 : parameter optimization using response surface methodology. *Inorganic Chemistry Communications*, pp: 149:1104.
18. Eskikaya O, Isik Z, Arslantas C, Yabalak E, Balakrishnan D, Dizge N, Rao KS, (2023). Preparation of hydrochar bio-based catalyst for fenton process in dye-containing wastewater treatment. *Environmental Research*, pp: 216:114357.
19. Yu H, Cai D, Li Sh, Gao C, Xue L, (2023). Tight UF membranes with ultrahigh water flux prepared by in-situ growing ZIF particles in NIPS process for greatly enhanced dye removal efficiency. *Journal of Membrane Science*, pp: 666:121136.
20. Zhu K, Mohammed S, Tang H, Xie Z, Fang S, Liu S, (2023). ZIF-67/SA@PVDF ultrafiltration membrane with simultaneous adsorption and catalytic oxidation for dyes. *Sustainability*, pp: 15:2879.
21. Thoa LThK, Thao TThPh, Nguyen-Thi M, Duc Chung N, Ooi ChW, Park SM, Lan TTh, Quang HT, Khoo KSh, Show PL, Duc Huy N, (2023) Microbial biodegradation of recalcitrant synthetic dyes from textile-enriched wastewater by fusarium oxysporum, *Chemosphere*, pp: 325:138392.
22. Selvan BK, Pandiyan R, Vaishnavi M, Das S, Thirunavoukkrasu M, (2023). Ameliorative biodegradation of hazardous textile industrial wastewater dyes by potential microalgal sp. *Biomass Conv. Bioref.*, pp:13:13481–13492.
23. Embaby MS, Elwany SD, Setyaningsih W, Saber MR, (2018). The adsorptive properties of UiO-66 towards organic dyes: a record adsorption capacity for the anionic dye alizarin red s. *Chin. J. Chem. Eng.*, pp: 26:731-739.
24. Chen Q, He Q, Lv M, Xu Y, Yang H, Liu X, Wei F, (2015). Selective adsorption of cationic dyes by UiO-66-NH₂. *Applied Surface Science*, pp: 327:77-85.
25. Couillard D, (1994). The use of peat in wastewater treatment. *Water Research*, pp: 28:1261-1274.
26. Bu X.H., Zaworotko M.J., Zhang Zh., *Metal-Organic Framework from Design to Applications*, first ed., Springer, Nature Switzerland, 2020.
27. Lin H, Jie B, Ye J, Zhai Y, Luo Zh, Shao G, Chen R, Zhang X, Yang Y, (2023). Recent advance of macroscopic metal-organic frameworks for water treatment: a review. *Surfaces and Interfaces*, pp: 36:102564.
28. Kaur H, Devi N, Siwal SS, Alsanie WF, Thakur MK, (2023). Metal–organic framework-based materials for wastewater treatment: superior adsorbent materials for the removal of hazardous pollutants. *ACS Omega*, pp: 8:9004–9030.
29. Tambat SN, Ahirrao DJ, Pandit AB, Jha N, Sontakke ShM, (2020). Hydrothermally synthesized N₂-UiO-66 for enhanced and selective adsorption of cationic dyes. *Environmental Technology & Innovation*, pp:19:101021.
30. Li Y, Liu Y, Gao W, Zhang L, Liu W, Jingjing L, Wang Z, Deng YJ, (2014). Microwave-assisted synthesis of UiO-66 and its adsorption performance towards dyes. *Cryst. Eng. Comm.*, pp: 16:7037–7042.
31. Zhang KD, Tsai FC, Ma N, Xia Y, Liu HL, Zhan XQ, Yu XY, Zeng XZ, Jiang T, Shi D, Chang CJ, (2017). Adsorption behavior of high stable Zr-based MOFs for the removal of acid organic dye from water. *Materials*, pp:10:205.

32. Tambat SN, Sane PK, Suresh S, Varadan ON, Pandit AB, Sontakke ShM, (2018). Hydrothermal synthesis of NH₂-UiO-66 and its application for adsorptive removal of dye. *Advanced Powder Technology*, pp: 29:2626-2632.
33. Mousavi AV, Ahmadipouya S, Shokrgozar A, Molavi H, Rezakazemi M, Ahmadijokani F, Arjmand M, (2021). Adsorption performance of UiO-66 towards organic dyes: effect of activation conditions. *Journal of Molecular Liquids*, pp: 321:114487.
34. Qiu J, Feng Y, Zhang X, Jia M, Yao J, (2017). Acid-promoted synthesis of UiO-66 for highly selective adsorption of anionic dyes: adsorption performance and mechanisms. *J. Colloid Interface Sci.*, pp: 499:151-158.
35. Molavi H, Hakimian A, Shojaei A, Raeiszadeh M, (2018). Selective dye adsorption by highly water stable metal-organic framework: long term stability analysis in aqueous media. *Appl. Surf. Sci.*, pp: 445:424-436.
36. Mohammadi A, Sedighi M, Afsari M, (2022). Optimization of the synthesis of UiO-66-NH₂ catalyst and its application for removing organophosphorus pesticides from wastewater. *J. Hydraul. Struct.*, pp: 8:1-16.
37. Yang J, Dai Y, Zhu X, Wang Z, Li Y, Zhuang Q, Shi J, Gu J, (2015). Metal-organic frameworks with inherent recognition sites for selective phosphate sensing through their coordination-induced fluorescence enhancement effect. *J. Mater. Chem. A*, pp: 3:7445-7452.
38. Guo Zh, Xiao Ch, Maligal-Ganesh RV, Zhou L, Goh TW, Li X, Tesfagaber D, Thiel A, Huang W, (2014). Pt-nanoclusters confined within metal-organic framework cavities for chemoselective cinnamaldehyde hydrogenation. *ACS Catal.*, pp: 4:1340-1348.
39. Forbes, E., Franks, G. V. (2013). Selective separation of hematite from quartz by flotation using a temperature responsive polymer. *Proceeding of the Iron Ore Conference, Perth, Australia*.
40. Abaka-Wood BG, Addai-Mensah J, Skinner W, (2017). A study of flotation characteristics of monazite, hematite, and quartz using anionic collectors. *International Journal of Mineral Processing*, pp: 158:55-62.
41. Yang Zh, Han Y, Teng Q, Zhang G, Liu Sh, (2023) Aggregation process of fine hematite particles suspension using xanthan gum in the presence of Fe (III). *Arabian Journal of Chemistry*, pp: 16:104539.
42. Fan G, Wang L, Cao Y, Li Ch, (2020). Collecting agent-mineral interactions in the reverse flotation of iron ore: a brief review. *Minerals*, pp: 10:681.
43. Shrimali K, Jin J, Vaziri Hassas B, Wang X, Miller JD, (2016). The surface state of hematite and its wetting characteristics. *J. Colloid Interface Sci.*, pp: 477:16-24.
44. Ishikawa K, Yoshioka T, Sato T, Okuwaki A, (1997). Solubility of hematite in LiOH, NaOH and KOH solutions. *Hydrometallurgy*, pp: 45:129-135.
45. Priyantha N, Lim LBL, Dahri MKh, Tennakoon DTB, (2013). Dragon fruit skin as a potential low-cost biosorbent for the removal of manganese (II) ions. *Journal of Applied Sciences in Environmental Sanitation*, pp: 8:179-188.
46. Dada AO, (2012). Langmuir, Freundlich, Temkin and Dubinin-Radushkevich isotherms studies of equilibrium sorption of Zn²⁺ onto phosphoric acid modified rice husk. *IOSR Journal of Applied Chemistry*, pp: 3:38-45.
47. Kara M, Yuzer H, Sabah E, Celik MS, (2007). Adsorption of cobalt from aqueous solutions onto sepiolite. *Water Res.*, pp: 37:224-232.



© 2024 by the authors. Licensee SCU, Ahvaz, Iran. This article is an open access article distributed under the terms and conditions of the Creative Commons Attribution 4.0 International (CC BY 4.0 license) (<http://creativecommons.org/licenses/by/4.0/>).

